A measurement of the energy loss spectrum of 150 GeV muons in iron

RD 34 Collaboration

E. Berger, R. Blair, J. Dawson, T. Fuess, V. Guarino, N. Hill, S. Magill, E. May, L. Nodulman, L. Price, J. Proudfoot, R. Stanek, D. Underwood, R. Wagner, B. Wicklund
Argonne National Laboratory, 9700 South Cass Avenue, Argonne IL 60439, USA

G. Blanchot, M. Bosman, P. Casado, M. Cavalli-Sforza, I. Efthymiopoulos, Yu. Ivanyushenkov, A. Juste, Ll. Miralles, S. Orteu, C. Padilla, J.A. Perlas, I. Riu, B. Ronceux, F. Teubert
Institut de Fisica d'Altes Energies, Universidad Autonoma de Barcelona, E-08193 Bellaterra (Barcelona), Spain

R. Arsenescu, S. Constantinescu, C. Blaj, V. Boldea, S. Dita
Institute of Atomic Physics, RO-Bucharest, Rumania

M. Cobal, O. Gildemeister, M. Nessi, A. Henriques, L. Poggioli, P. Sonderegger, G. Karapetian
CERN, CH-1211 Geneva 23, Switzerland

K. Anderson, E. Blucher, H. Evans, F. Merritt, J. Pilcher, H. Sanders, M. Shochet, F. Tang, A. Turcot, D. Wagner
University of Chicago, 5640 South Ellis Avenue, Chicago IL 60637, USA

Z. Ajaltouni, F. Badaud, N. Bouhemaid, P. Brette, M. Brossard, R. Chadelas, J.-C. Chevaleyre, M. Crouau, F. Daudon, J.-J. Dugne, B. Michel, G. Montarou, G.S. Muanza, D. Pallin, H. Plothow-Besch, S. Poirot, G. Reinmuth, L.-P. Says, F. Vazeille
LPC Clermont–Ferrand, Université Blaise Pascal / CNRS–IN2P3, F-63177 Aubière Cedex, France

A. Astvatsaturov, O. Borisov, J. Budagov, I. Chirikov-Zorin, G. Chlachidze, V. Glagolev, S. Kakurin, V. Kolomoets, V. Kovtun, V. Kukhtin, A. Lebedev, I. Liba, O. Lomakina, Yu. Lomakin, S. Malyukov, I. Minashvili, D. Pantea, O. Pukhov, V. Romanov, N. Russakovich, V. Senchishin, A. Semenov, A. Sissakian, A. Shchelchkov, V. Shevtsov, S. Studenov, S. Tokar, N. Topilin, V. Vinogradov, S. Vorozhtsov, G. Yarygin
JINR Dubna, RU-141980 Dubna, Moscow Region, Russia

F. Cogswell, R. Downing, D. Errede, S. Errede, M. Haney, V. Simaitis, J. Thaler
University of Illinois, PO Box 4348, Chicago IL 60680, USA

P. Amaral[a], A. Amorim[a], J. Carvalho[b], M. David[a], A. Gomes[a], A. Maio[a], J. P. Martins[a], A. Onofre[b], H. Wolters[c]
[a]LIP and FCUL-University Lisbon, [b]LIP and FCTUC-University Coimbra, [c]University Cat. Figueira da Foz, P-1700 Lisboa, Portugal

C. Bromberg, J. Huston, R. Miller, R. Richards, C. Yosef
Michigan State University, East Lansing, MI 48824-1321, USA

A. Alifanov, A. Bogush, V. Golubev, V. Rumyantsev, Y. Kulchitsky
Institute of Physics ASB, Minsk, Belarus

C. Angelini, D. Autiero, V. Cavasinni, D. Costanzo, A. De Santo, T. Del Prete, B. Di Girolamo, V. Flaminio, S. Lami, C. Lazzeroni, E. Mazzoni, G. Renzoni
Pisa University and INFN, I-56010 Pisa, Italy

T. Davidek, J. Dolejsi, Z. Dolezal, R. Leitner, K. Soustruznik, M. Suk, P. Tas, Z. Trka, S. Valkar, M. Zdrazil
Charles University, CZ-18000 Praha 8, Czech Republic

M. Lokajicek, S. Nemecek
Academy of Science, CZ-18040 Praha 8, Czech Republic

A. Karyukhin, V. Klyukhin, Yu. Khokhlov, S. Kopikov, M. Kostrikov, M. Kulagin, V. Lapin, Y. Protopopov, V. Sidorov, A. Solodkov, E. Starchenko, A. Surkov, A. Zaitsev
Institute for High Energy Physics, Protvino, Russia

L. Caloba, M. Gaspar, F. Marroquin, A. Pereira, J.M. Seixas, COPPE/EE/UFRJ, Rio de Janeiro, Brazil

S. Berglund, C. Bohm, E. Johansson, S. Hellman, S. Holmgren, K. Jon-And, B. Sellden, S. Tardel, N. Yamdagni
Stockholm University, S-11346 Stockholm, Sweden

A. Ferrer, P.F. Honoré, F. Albiol
IFIC Valencia, E-46100 Burjassot (València), Spain

K. De, E. Gallas, J. Li, L. Sawyer, R. Stephens, M. Turcotte, A. White
University of Texas at Arlington, USA

H. Hakopian, V. Grabsky, E. Mnatsakanian, A. Vartapetian
Yerevan Physics Institute, Alikhanian Brothers Street 2, AM-375036 Yerevan 36, Armenia

Abstract. The energy loss spectrum of 150 GeV muons has been measured with a prototype of the ATLAS hadron calorimeter in the H8 beam of the CERN SPS. The differential probability dP/dv per radiation length of a fractional energy loss $v = \Delta E_\mu / E_\mu$ has been measured in the range $v = 0.01 \div 0.95$; it is compared with the theoretical predictions for energy losses due to bremsstrahlung and production of electron–positron pairs or of energetic knock-on electrons. The integrated probability $\int_{0.01}^{0.95}(dP/dv)dv$ is $(1.610 \pm 0.015_{\text{stat}} \pm 0.105_{\text{syst}}) \cdot 10^{-3}$ in agreement with the theoretical predictions $1.556 \cdot 10^{-3}$ and $1.619 \cdot 10^{-3}$. Agreement with theory is also found in two intervals of v where production of electron–positron pairs and knock-on electrons dominates. In the region of bremsstrahlung dominance ($v = 0.12 \div 0.95$) the measured integrated probability $(1.160 \pm 0.040_{\text{stat}} \pm 0.075_{\text{syst}}) \cdot 10^{-4}$ is in agreement with the theoretical value of $1.185 \cdot 10^{-4}$, obtained using the Petrukhin and Shestakov description of the bremsstrahlung process. The same result is about 3.6 standard deviations (defined as the quadratic sum of statistical and systematic errors) lower than the theoretical prediction of $1.472 \cdot 10^{-4}$, obtained using Tsai's description of bremsstrahlung.

1 Introduction

The search for heavy Higgs bosons via their decay to Z and W pairs at the Large Hadron Collider requires the detection of muons with energies in excess of 100 GeV. It is well known that in this regime the energy loss of muons in iron or higher Z materials is dominated by radiative effects. In the ATLAS [1] detector muons will be measured by tracking chambers within a toroidal air-core magnet after they have crossed more than 100 radiation lengths of material in the electromagnetic and hadronic calorimeters. It is therefore useful to check precisely the theoretical predictions for muon energy losses in such materials.

Energy losses of muons at very high energies, up to 10 TeV, have been measured in cosmic-ray experiments [2–4]. In these experiments muon energies were measured with a magnetic spectrometer and reasonable agreement between data and calculations was found, except in the region of very small energy losses [4].

Energy losses of muons up to 200 GeV were measured in various accelerator experiments. The measurements by the European Muon Collaboration [5] are in the region of bremsstrahlung dominance and good agreement was found with Tsai's [6] description of this process. The data of the BCDMS Collaboration [7] as well as the results of the Siegen group [8] agree well with calculations [9] based on the Kokoulin and Petrukhin [10] pair-production formula and the Petrukhin and Shestakov [11] expression for bremsstrahlung. It was pointed out by Tannenbaum [12] that Tsai's description of bremsstrahlung differs from the Petrukhin and Shestakov calculations by approximately 20%. In the same paper the lack of precise measurements in the region of bremsstrahlung dominance (large fractional energy losses) is mentioned.

In this paper, a measurement performed in 1995 with 150 GeV muons incident on a prototype of the ATLAS Tile Calorimeter is described and the results are compared with theoretical predictions. For 150 GeV muons, the dominant energy loss process in the region from 1.5 to 5 GeV is expected to be electron–positron pair production, while energetic knock-on electrons dominate from 5 to 20 GeV, and photons from bremsstrahlung dominate the loss spectrum above 20 GeV. Therefore measuring the spectrum between
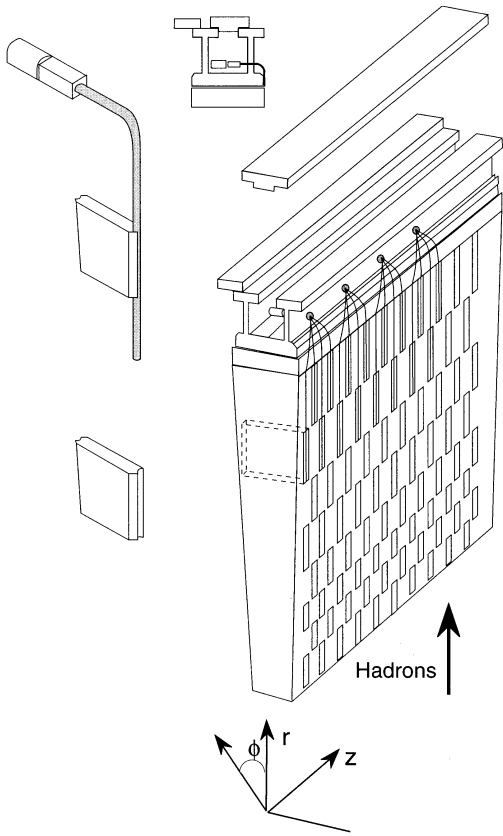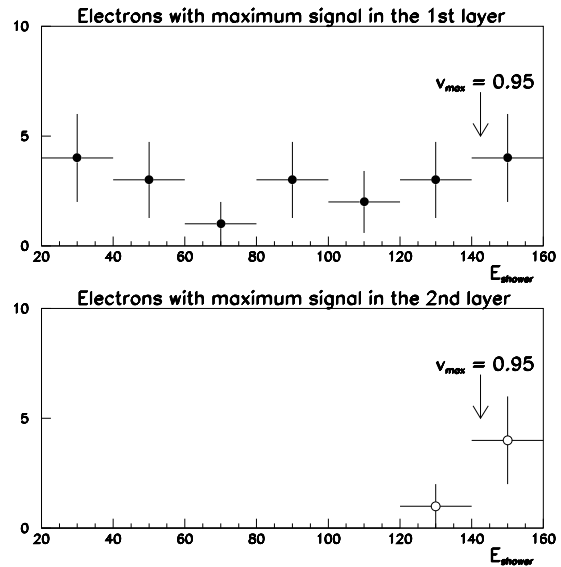
Fig. 1. Principle of the ATLAS Tile Calorimeter module. The direction of secondary particles produced in future LHC pp collisions is shown by the arrow Hadrons. In the experiment described, muons cross the tiles at perpendicular incidence along z direction

Fig. 2. Spectrum of the electron contamination of the muon beam

1.5 and 150 GeV allows one to check the contributions from all three processes.

2 Experiment and data analysis

The ATLAS Tile Calorimeter is an iron-scintillator sampling calorimeter equipped with wavelength-shifting fibre readout. An important feature of this calorimeter is that the scintillator tiles are placed perpendicular to the colliding beams; a detailed description of the calorimeter concept and of the prototypes is given elsewhere [13]. For the purpose of this measurement, the calorimeter was placed in the H8 beam of the CERN SPS, and oriented so that particles cross the tiles at perpendicular incidence (along the z-axis on Fig. 1). In this configuration the muon beam traverses alternating layers of iron (14 mm) and scintillator (3 mm); this relatively fine granularity gives a resolution of $\sigma/E = 24\%/\sqrt{(E[\text{GeV}])}$ for electromagnetic showers. The fibres collecting light from the scintillator are read out by photomultipliers and are grouped in such a way that five calorimeter layers are defined. Each layer is approximately 20 cm thick and contains 8.8 radiation lengths (X_0) of iron. In the experimental set-up, five calorimeter modules were stacked on top of each other, and the beam entered in the centre of the second, the third (central), or the fourth module. Walls of scintillator detectors [14] were placed on the upstream and downstream sides of the calorimeter.

Particles of the momentum-analysed muon beam, with an energy $E_\mu = 150$ GeV, were triggered by three scintillator hodoscopes; the direction of incidence was measured by a pair of two-coordinate wire chambers. Approximately 550 000 muon triggers were used in this analysis.

A minimum-ionizing particle signal was required in scintillator hodoscopes and in the upstream scintillator wall in order to suppress trigger more than one entering particle. Hadron contamination was eliminated by cuts on the impact point and on the divergence of the beam together with the requirement that more than 95% of the signal be contained in the module traversed by the beam.

The electron contamination of the beam from muon decay was estimated to be negligible because the mean decay length of 150 GeV muons to electrons is about 10^6 m. The energy spectrum of electron candidates defined as events with zero signals (compatible with pedestals) in the last layer ($35.2 \div 44\ X_0$) of the calorimeter and in the downstream scintillator wall is shown on Fig. 2. As expected, the electron contamination is very low and its maximum signal is in the first layer of the calorimeter. A few events with energies of about 150 GeV having maximum signal in the second layer were also found in the data. The number of events is compatible with the GEANT Monte Carlo prediction that about 70% of electron-induced showers with an energy of 150 GeV give maximum signal in the first layer of the calorimeter and 30% of showers have a maximum in the second layer. After the contamination cuts, a sample of about 465 000 muon events is left.

In order to ensure full containment of electromagnetic showers produced by muon radiation or knock-on electrons and to suppress the electron background, only events with maximum response in the second or third layer (seen by the beam) of the calorimeter were selected and $v_{\text{max}} = 0.95$ (142.5 GeV) was set as the upper limit of the studied interval of fractional losses. In order to calculate the effective

458
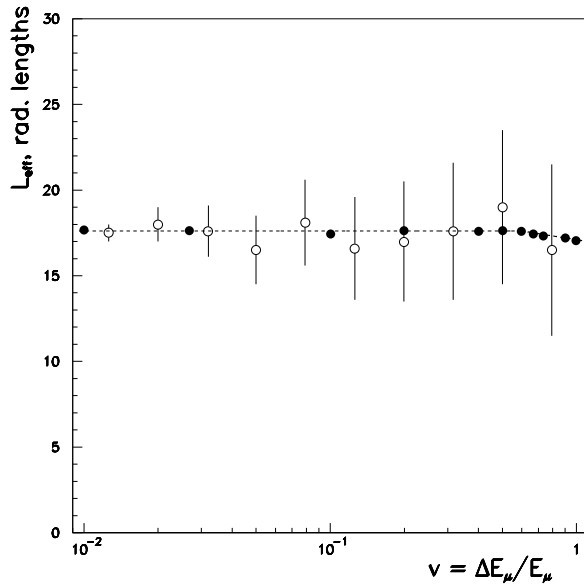
Fig. 3. The length L_{eff} (in radiation lengths of iron) of the muon path in the calorimeter over which showers are accepted by the selection algorithm, as a function of the relative muon energy losses. *Full* and *empty circles* are results of simplified and GEANT Monte Carlo calculations, respectively

Fig. 4. Example of a 36 GeV electromagnetic shower as seen in the data. The energy E_{shower} is the sum of energies in three consecutive layers (second to fourth) with the signal above $E_{\text{mp}}+3\sigma_{\text{mp}}$ and with the most probable muon signal E_{mp} subtracted. The arrow corresponds to the direction of the incident muon

length L_{eff} over which showers with energy E_{shower} (measured as described below) would be accepted with this selection method, the earliest and latest starting points (x_{min} and x_{max}) of showers with the largest signal in the second or third layer were calculated using a well-known parametrization [15] of the longitudinal profile of the energy deposition of electromagnetic showers
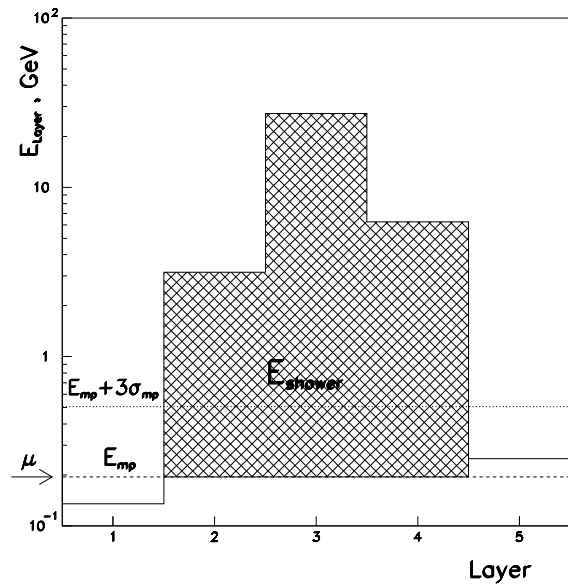
$$\mathrm{d}E/\mathrm{d}x \propto x^{\alpha(E_{\text{shower}})} \cdot e^{-\beta(E_{\text{shower}})x} \ .$$

The difference $L_{\text{eff}}(E_{\text{shower}}) = (x_{\text{max}} - x_{\text{min}})/X_0$ is shown in Fig. 3 as a function of the fractional energy loss $v = \Delta E_\mu/E_\mu$; it can be seen that L_{eff} is rather precisely given by the thickness of two calorimeter layers (17.6 X_0) up to about 90 GeV ($v = 0.6$), while for higher energy losses the effective length decreases (due to the logarithmic longitudinal growth of showers) by at most 3%. L_{eff} above 90 GeV is well described by

$$L_{\text{eff}}(E_{\text{shower}}) = 17.6 - \ln(E_{\text{shower}}[\text{GeV}]/90)$$

Acceptance calculations were cross-checked by GEANT 3.21 Monte Carlo simulations (which include muon radiative losses and knock-on electron production); the simulations confirm the analytical result, with larger errors for large muon energy losses.

The energy E_{shower} lost by muons in the calorimeter is defined in this analysis by excluding the minimum-ionization signal. It was calculated by summing the signals in two to four consecutive layers and subtracting the experimental value of the most probable muon signal E_{mp} in those layers. All consecutive layer signals in excess of $E_{\text{mp}} + 3\sigma_{\text{mp}}$ were summed to obtain E_{shower} (see Fig. 4). This method minimizes the correction from the low-energy ionization produced by muons and the error from its fluctuation. These corrections are important for the lowest energy losses: for

instance, for $E_{\text{shower}} = 1.5$ GeV the muon ionization signal is almost $0.3E_{\text{shower}}$ therefore it is imperative to subtract it from the total signal.

The subtraction procedure was also simulated using GEANT 3.21, in order to estimate the contribution of events with more than one shower to the differential probability distribution. One hundred thousand muons traversing the calorimeter structure were simulated; for each event the energy lost by muons in each of 55 iron and scintillator slabs together with the energy losses of electrons and positrons in the scintillators were recorded. Differential probability distributions obtained by forming the E_{shower} sum with different subtraction procedures were compared with the distribution of the largest single energy loss in one iron slab (0.8 X_0), because the latter distribution can be directly compared with the theoretical results. After subtracting E_{mp} the expected contribution of multiple shower events to $\mathrm{d}P/\mathrm{d}v$ is 25%, 6%, and 0% for $v = 0.01, 0.1$, and 1. respectively, as shown in Fig. 5. In the figure one may also see that subtraction of a truncated mean of the muon signal (1.6 times the most probable signal) fully eliminates multiple shower contributions.

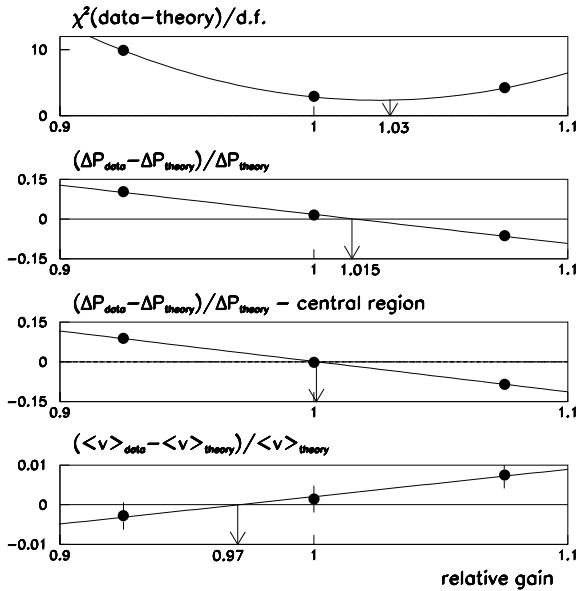Two different methods for the definitions of ΔE_μ:
• $\Delta E_\mu = E_{\text{shower}}$ with the subtraction of the most probable signal followed by the correction of $\mathrm{d}P/\mathrm{d}v$, and
• $\Delta E_\mu = E_{\text{shower}}$ with the subtraction of the truncated mean signal
have been used to analyse the data. The two methods give a difference in the total integrated energy loss probability of $\pm 0.3\%$ which was included in the estimate of the systematic error.
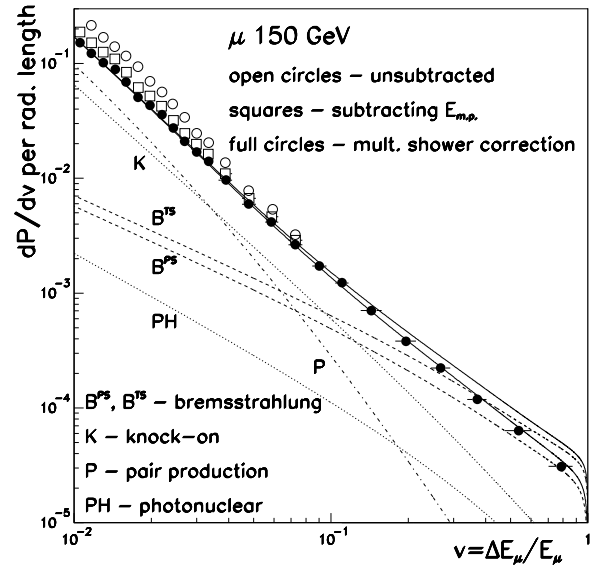
The signal energy scale, *i.e.* the conversion factor used to obtain the energy of the signals from the digitized photomultiplier signals, was not independently known to sufficient
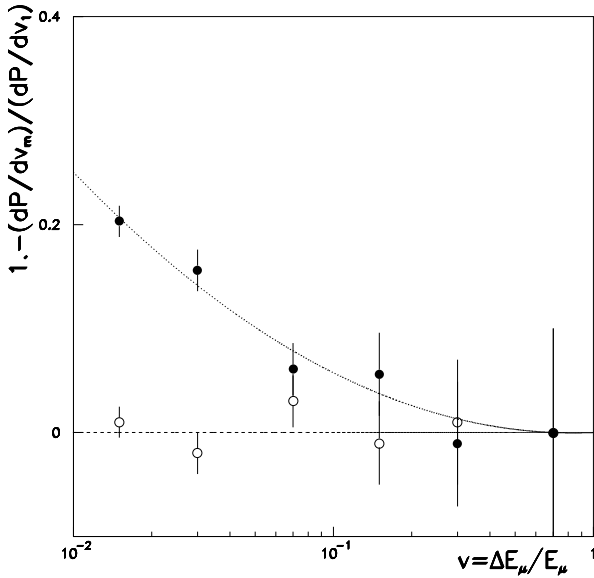
Fig. 5. Monte Carlo study of the multiple shower contribution to the differential probability distribution $\mathrm{d}P/\mathrm{d}v$. The full circles correspond to fractional losses defined as $v_\mathrm{m} = (\Delta E_\mu - E_\mathrm{mp})/E_\mu$, empty circles are for $v_\mathrm{m} = (\Delta E_\mu - 1.6 \cdot E_\mathrm{mp})/E_\mu$. The energy loss in one radiative or knock-on process is defined as $v_1 = \Delta E_\mathrm{max}/E_\mu$ with ΔE_max being the largest energy loss in one iron slab ($0.8\ X_0$) in each muon's crossing of the calorimeter

Fig. 7. The distribution of differential probabilities $\mathrm{d}P/\mathrm{d}v$ for the energy loss of 150 GeV muons in iron. The curves P, K, B^PS and B^TS for pair production, knock-on electrons production and bremsstrahlung correspond to Eqs. (1), (2), (3) and (5) in the text. The full curves are the sum of P, K, and B^PS (lower one) and P, K, and B^TS (upper one). The contribution of the energy loss due to photonuclear reactions (PH) is also shown

Fig. 6. Determination of the energy scale conversion factor. The plots correspond to four different methods described in the text. The data are compared with the mean values of the two used theoretical predictions. The comparison is made at different values of the energy scale conversion factor. The results are plotted as *full circles* and they are fitted by quadratic and linear functions in order to obtain the values of the conversion factor shown by the arrows. The values of the energy scale conversion factor are in relative units – the value of 1 corresponds to the value of 6.15 pC/GeV used in the analysis

accuracy and was therefore obtained from the data by several methods (see Fig. 6).

- The signal/energy conversion factor was varied to obtain the best fit to the theoretical distribution of muon energy losses (see Sect. 3). The main effect of this procedure is to set the energy of the end-point of the experimental distribution to the muon beam energy; the conversion factor thus obtained is quite insensitive to the integral of the energy loss spectrum and its detailed shape.
- The conversion factor was calculated by requiring that the integral of the spectrum agree with theory.
- In the central region between 7.5 and 30 GeV ($v = 0.05$ to 0.2) where the data corrections are low and the difference between theoretical descriptions is still below $\pm 3\%$, the integrated probability was adjusted to its theoretical value.
- The mean energy loss in the central region of v was fitted to the theoretical prediction. This method is insensitive to the common normalization factor.

To minimize the dependence of results on theory, the mean value of the conversion factor obtained by the first and the last methods was used in the analysis. The other methods gave conversion factors differing by $\pm 3\%$. This value was used for the estimate of systematic errors.

The lower limit of the analysed energy loss spectrum was set to 1.5 GeV because for this value the signal from the processes studied in this paper is sufficiently well separated from the most probable muon signal:

$$E_\mathrm{mp} + 3\sigma_\mathrm{mp} \leq E_\mathrm{shower} - 3\sigma_\mathrm{shower} ,$$
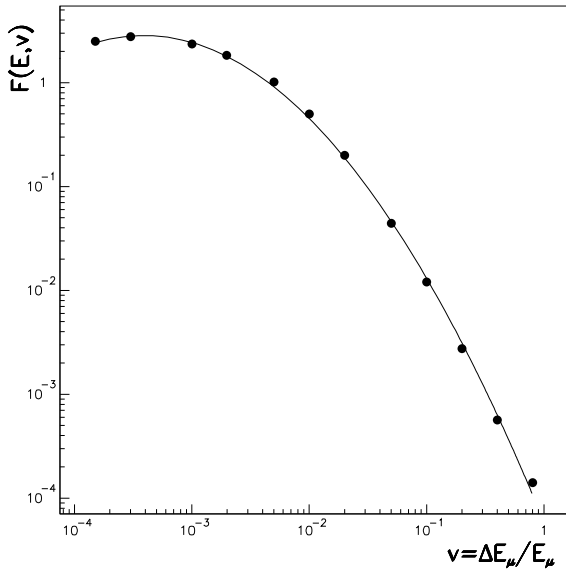
Fig. 8. The function $F(E_\mu, v)$ (see formula (1) in the text) for e^+e^- pair production by 150 GeV muons in iron. The points have been obtained by interpolation of values tabulated in [16]

where $\sigma_{\text{shower}}[\text{GeV}] = 0.24 \cdot \sqrt{E_{\text{shower}}[\text{GeV}]}$) for $E_{\text{shower}} \geq 1.5$ GeV.

Finally the differential probability per radiation length of a fractional energy loss in the i-th interval was calculated as

$$\frac{\Delta P}{\Delta v} = \frac{(N_i/N_{\text{tot}})}{\Delta v_i} \cdot \frac{1}{L_{\text{eff}}(\langle v \rangle_i)},$$

where N_i is the number of events in the i-th interval, N_{tot} is the total number of events passing the cuts, Δv_i is the width of the i-th interval, $L_{\text{eff}}(\langle v \rangle_i)$ is the effective length for the mean $\langle v \rangle_i$ of that interval.

The measured differential probabilities per radiation length of iron are given in Table 1 and are plotted in Fig. 7. The errors quoted are statistical only. The systematic errors of the energy loss spectrum are dominated by the uncertainty on the signal energy scale, which we take to be $\pm 3\%$, by the uncertainty on the muon energy ($\pm 1.5\%$), and by the uncertainty on the iron absorber thickness ($\pm 1.0\%$). Because the systematic errors are correlated, the data have been processed with different values of the signal energy scale, of the muon energies, and of absorber thickness. The maximal positive and negative deviations of mean values were taken as systematic errors. The result is an overall systematic error on the differential probability of fractional energy loss dP/dv of $\pm 7\%$, which dominates the results in the low-energy region, but is comparable to the statistical errors in the high-energy region.

3 Theoretical predictions

The theoretical predictions to be compared with these results are discussed next. The analytical expressions are given in full in order to facilitate comparison.

Pair production: The Kel'ner and Kotov expression [16] for the differential probability per radiation length of muon energy loss by pair production is

$$\left(\frac{dP}{dv}\right)_{\text{pair}} = C\frac{16}{\pi} Z^2 \alpha^2 \frac{1}{v} F(E_\mu, v) . \tag{1}$$

The constant C is given by $C = X_0 \rho N_A r_e^2 / A = 1.185 \cdot 10^{-2}$. Here N_A is the Avogadro constant, r_e is the classical electron radius and α is the fine structure constant; X_0, ρ, A and Z are the radiation length, the density, the atomic weight, and the atomic number of iron. The function $F(E_\mu, v)$ is tabulated in [16] for lead and sodium at different muon energies. The interpolation of Kel'ner and Kotov's function $F(E_\mu, v)$ for the energy loss of 150 GeV muons in iron is shown on Fig. 8 together with the parametrization used in this paper:

$$\ln F_{\text{Fe}}(E_\mu = 150 \text{ GeV}, v) = -0.175 \ln^2(v)$$
$$-2.748 \ln(v) - 9.736 .$$

Knock-on electrons: In order to describe the production of energetic knock-on electrons, the Bhabha formula [17] given by Rossi [18] is used (m_e is the electron mass and C as defined as above):

$$\left(\frac{dP}{dv}\right)_{\text{knock-on}} = C2\pi Z \left(\frac{m_e}{E_\mu}\right) \frac{1 - v + \frac{v^2}{2}}{v^2} . \tag{2}$$

Bremsstrahlung: In order to compare these results with predictions of muon bremsstrahlung, the expression given by Petrukhin and Shestakov [11], and another calculation by Tsai [6] are used.

The expression of Petrukhin and Shestakov

$$\left(\frac{dP}{dv}\right)^{\text{PS}}_{\text{bremsstrahlung}} =$$
$$C4Z^2\alpha \left(\frac{m_e}{m_\mu}\right)^2 \frac{1}{v} \left(\frac{4}{3} - \frac{4}{3}v + v^2\right) \Phi^{\text{PS}}(\delta) \tag{3}$$

contains the screening function:

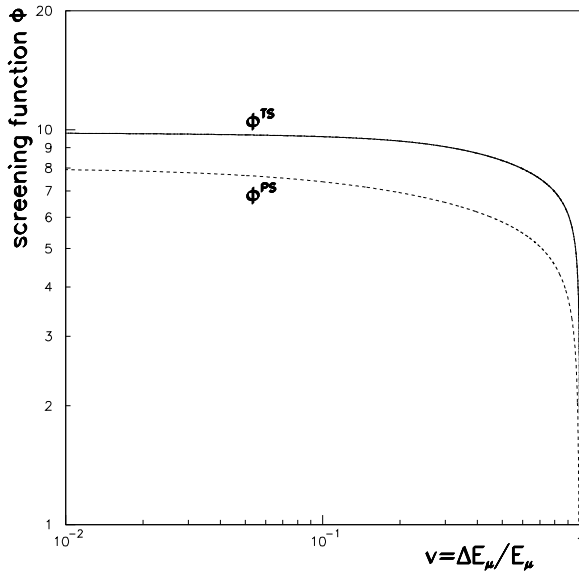$$\Phi^{\text{PS}}(\delta) = \ln \frac{(2/3)189(m_\mu/m_e)Z^{-2/3}}{1 + 189\sqrt{e}(\delta/m_e)Z^{-1/3}} , \tag{4}$$

where m_μ is the muon mass, $\delta = m_\mu^2 v/2E_\mu(1-v)$ is the minimum momentum transfer to the nucleus and $e = 2.718$. The function $\Phi^{\text{PS}}(\delta)$ is an approximation of the exact screening function and is valid within 1% up to $\delta = 0.1 m_\mu$ ($v = 0.9$ for $E_\mu = 150$ GeV) [11].

In order to compare the previous formula with the differential probability distribution given by Tsai [6, 12], his formula has been written as:

$$\left(\frac{dP}{dv}\right)^{\text{TS}}_{\text{bremsstrahlung}} =$$
$$C4Z^2\alpha \left(\frac{m_e}{m_\mu}\right)^2 \frac{1}{v} \left(\frac{4}{3} - \frac{4}{3}v + v^2\right) \Phi^{\text{TS}}(\delta) , \tag{5}$$

where the screening function $\Phi^{\text{TS}}(\delta)$ is:

$$\Phi^{\text{TS}}(\delta) = \frac{\phi_1(a\delta)}{4} - \frac{1}{3}\ln Z - f_{\text{coul}} + \frac{1}{Z}\left(\frac{\psi_1(a'\delta)}{4} - \frac{2}{3}\ln Z\right)$$
$$+ \frac{\frac{2}{3}(1-v)}{\frac{4}{3} - \frac{4}{3}v + v^2}\left(\frac{\phi_1 - \phi_2}{4} + \frac{1}{Z}\frac{\psi_1 - \psi_2}{4}\right) . \tag{6}$$

Fig. 9. Comparison of screening functions of the Petrukhin and Shestakov (Φ^{PS}) and the Tsai (Φ^{TS}) description of bremsstrahlung of 150 GeV muons in iron

Fig. 10. Detailed comparison of the data and theory with the Petrukhin and Shestakov xdescription of bremsstrahlung. Hatched and empty rectangles correspond to statistical and systematic errors, respectively. The upper curve is the theoretical prediction with Tsai's formula for bremsstrahlung

The functions ϕ_1 and ψ_1 have arguments $a\delta$ and $a'\delta$; $a = 184.15/(\sqrt{e}\, m_{\mathrm{e}} Z^{1/3})$ and $a' = 1194/(\sqrt{e}\, m_{\mathrm{e}} Z^{2/3})$. The two functions are defined for zero-momentum transfer as:

$$\phi_1(0) = 4\ln(\sqrt{e}\, a Z^{1/3} m_\mu) \quad \text{and} \quad \psi_1(0) = 4\ln(\sqrt{e}\, a' Z^{2/3} m_\mu)$$

and for an arbitrary δ as:

$$\phi_1(a\delta) = \phi_1(0) - 2\ln(1 + (a\delta)^2) - 4(a\delta)\mathrm{arctg}(1/a\delta),$$
$$\psi_1(a'\delta) = \psi_1(0) - 2\ln(1 + (a'\delta)^2) - 4(a'\delta)\mathrm{arctg}(1/a'\delta).$$

The functions ϕ_2 and ψ_2 are related to the functions ϕ_1 and ψ_1 by the equations from [6]:

$$\phi_2(a\delta) = \phi_1(a\delta) - (2/3)/(1 + 6.5a\delta + 6(a\delta)^2),$$
$$\psi_2(a'\delta) = \psi_1(a'\delta) - (2/3)/(1 + 40a'\delta + 400(a'\delta)^2).$$

These equations fix the asymptotic behaviour of ϕ_2 and ψ_2:

$$\phi_1(0) - \phi_2(0) = \psi_1(0) - \psi_2(0) = 2/3$$

at zero momentum transfer and

$$\phi_1 - \phi_2 = \psi_1 - \psi_2 = 0$$

for large arguments.
Finally $f_{\mathrm{coul}} = 4.197\cdot 10^{-2}$ is the correction for the Coulomb interaction.
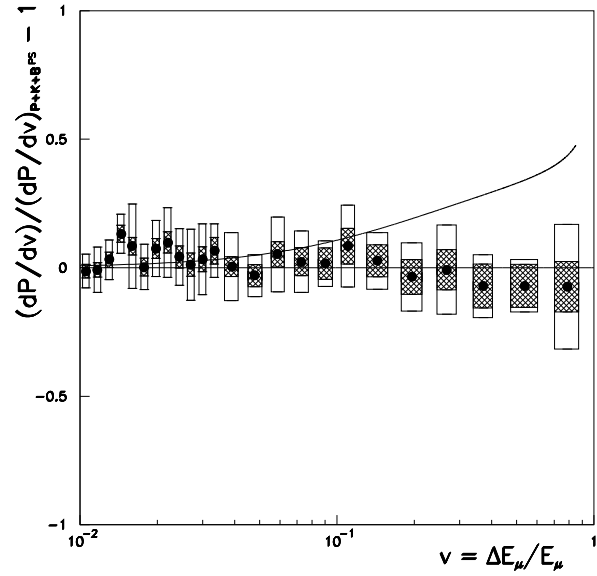
Screening functions for both the Petrukhin and Shestakov (Φ^{PS}) and the Tsai (Φ^{TS}) description of bremsstrahlung are plotted on Fig. 9.

Photonuclear interactions: Photonuclear interactions contribute also to the muon energy loss. The probability calculated by Bezrukov and Bugaev [19] is given by the formula from Ref. [9]:

$$\left(\frac{\mathrm{d}P}{\mathrm{d}v}\right)_{\mathrm{photonuclear}} = C\left(\frac{A\sigma_{\gamma N}(\epsilon)}{\pi r_{\mathrm{e}}^2}\right)\frac{\alpha}{2}v\Gamma(E_\mu, v), \qquad (7)$$

where the function $\Gamma(E_\mu, v)$ is given by

$$\Gamma(E_\mu, v) = \frac{3}{4}G(x)\left(\kappa\ln(1 + \frac{m_1^2}{t}) - \frac{\kappa m_1^2}{m_1^2 + t} - \frac{2m_\mu^2}{t}\right)$$

$$+ \frac{1}{4}\left(\kappa\ln(1 + \frac{m_2^2}{t}) - \frac{2m_\mu^2}{t}\right)$$

$$+ \frac{m_\mu^2}{2t}\left(\frac{3}{4}G(x)\frac{m_1^2}{m_1^2 + t} + \frac{1}{4}\frac{m_2^2}{t}\ln(1 + \frac{t}{m_2^2})\right) \qquad (8)$$

with

$$G(x) = \frac{3}{x^2}\left(\frac{x^2}{2} - 1 + e^{-x}(1 + x)\right)$$

$$x = 0.00282A^{1/3}\sigma_{\gamma N}(\Delta E_\mu)$$

$$\sigma_{\gamma N}(\Delta E_\mu) = 114.3 + 1.647\ln^2(0.0213\Delta E_\mu[\mathrm{GeV}])\ \mu b$$

$$t = \frac{m_\mu^2 v^2}{1 - v}$$

$$\kappa = 1 - \frac{2}{v} - \frac{2}{v^2}$$

$$m_1^2 = 0.54\ \mathrm{GeV}^2$$

$$m_2^2 = 1.80\ \mathrm{GeV}^2\ .$$

The contribution of photonuclear interactions is about 1% for the lowest values of the fractional loss v and about 5% for the highest v value (see Fig. 7), but it is suppressed by the selection criteria applied to the data which have been optimized for electromagnetic secondary products. The maximum contributions of photonuclear processes are estimated to be about 0.5% and 2% for the lowest and the highest values of v, respectively, and have been subtracted from the measured values of $\mathrm{d}P/\mathrm{d}v$.

The values of these theoretical expressions over the observed energy-loss range are given in Fig. 7; the sum of the differential probabilities from the first three processes are given in the figure and in Table 1. The data can be compared with the calculations of Kel'ner and Kotov for pair produc-

Table 1. Comparison of the measured differential probability values $\Delta P/\Delta v$ for fractional muon energy losses with theoretical calculations $(\mathrm{d}P/\mathrm{d}v)_{P+K+B}^{\mathrm{PS}}$ according to the addition of formulae (1), (2) and (3) and $(\mathrm{d}P/\mathrm{d}v)_{P+K+B}^{\mathrm{TS}}$ according to the addition of formulae (1), (2) and (5) in the text. Only statistical errors are quoted. The error of $\langle v \rangle$ is estimated as the r.m.s. value divided by the square root of the number of events in a given interval

$\langle v \rangle$	$\Delta P/\Delta v$	$(\mathrm{d}P/\mathrm{d}v)_{P+K+B^{\mathrm{PS}}}$	$(\mathrm{d}P/\mathrm{d}v)_{P+K+B^{\mathrm{TS}}}$
$(1.054 \pm 0.001) \times 10^{-2}$	$(1.50 \pm 0.04) \times 10^{-1}$	1.52×10^{-1}	1.54×10^{-1}
$(1.170 \pm 0.001) \times 10^{-2}$	$(1.22 \pm 0.03) \times 10^{-1}$	1.23×10^{-1}	1.24×10^{-1}
$(1.298 \pm 0.001) \times 10^{-2}$	$(1.02 \pm 0.03) \times 10^{-1}$	0.99×10^{-1}	1.00×10^{-1}
$(1.441 \pm 0.001) \times 10^{-2}$	$(9.0 \pm 0.3) \times 10^{-2}$	7.93×10^{-2}	8.03×10^{-2}
$(1.600 \pm 0.002) \times 10^{-2}$	$(6.9 \pm 0.2) \times 10^{-2}$	6.37×10^{-2}	6.45×10^{-2}
$(1.781 \pm 0.002) \times 10^{-2}$	$(5.1 \pm 0.2) \times 10^{-2}$	5.07×10^{-2}	5.15×10^{-2}
$(1.975 \pm 0.002) \times 10^{-2}$	$(4.4 \pm 0.2) \times 10^{-2}$	4.07×10^{-2}	4.14×10^{-2}
$(2.192 \pm 0.003) \times 10^{-2}$	$(3.6 \pm 0.1) \times 10^{-2}$	3.26×10^{-2}	3.32×10^{-2}
$(2.438 \pm 0.003) \times 10^{-2}$	$(2.7 \pm 0.1) \times 10^{-2}$	2.59×10^{-3}	2.65×10^{-3}
$(2.702 \pm 0.004) \times 10^{-2}$	$(2.11 \pm 0.09) \times 10^{-2}$	2.08×10^{-2}	2.13×10^{-2}
$(2.996 \pm 0.004) \times 10^{-2}$	$(1.71 \pm 0.08) \times 10^{-2}$	1.67×10^{-2}	1.71×10^{-2}
$(3.333 \pm 0.005) \times 10^{-2}$	$(1.41 \pm 0.07) \times 10^{-2}$	1.32×10^{-2}	1.37×10^{-2}
$(3.886 \pm 0.009) \times 10^{-2}$	$(9.6 \pm 0.4) \times 10^{-3}$	9.54×10^{-3}	9.90×10^{-3}
$(4.81 \pm 0.01) \times 10^{-2}$	$(5.9 \pm 0.3) \times 10^{-3}$	6.08×10^{-3}	6.37×10^{-3}
$(5.89 \pm 0.02) \times 10^{-2}$	$(4.1 \pm 0.2) \times 10^{-3}$	3.98×10^{-3}	4.22×10^{-3}
$(7.28 \pm 0.02) \times 10^{-2}$	$(2.6 \pm 0.1) \times 10^{-3}$	2.57×10^{-3}	2.77×10^{-3}
$(9.02 \pm 0.03) \times 10^{-2}$	$(1.7 \pm 0.1) \times 10^{-3}$	1.68×10^{-3}	1.84×10^{-3}
$(1.105 \pm 0.004) \times 10^{-1}$	$(1.22 \pm 0.08) \times 10^{-3}$	1.13×10^{-3}	1.27×10^{-3}
$(1.440 \pm 0.008) \times 10^{-1}$	$(7.1 \pm 0.4) \times 10^{-4}$	6.89×10^{-4}	7.92×10^{-4}
$(1.96 \pm 0.01) \times 10^{-1}$	$(3.8 \pm 0.3) \times 10^{-4}$	3.94×10^{-4}	4.69×10^{-4}
$(2.68 \pm 0.02) \times 10^{-1}$	$(2.2 \pm 0.2) \times 10^{-4}$	2.27×10^{-4}	2.80×10^{-4}
$(3.71 \pm 0.03) \times 10^{-1}$	$(1.2 \pm 0.1) \times 10^{-4}$	1.29×10^{-4}	1.65×10^{-4}
$(5.38 \pm 0.06) \times 10^{-1}$	$(6.4 \pm 0.6) \times 10^{-5}$	6.75×10^{-5}	9.06×10^{-5}
$(7.87 \pm 0.09) \times 10^{-1}$	$(3.1 \pm 0.3) \times 10^{-5}$	3.49×10^{-5}	5.02×10^{-5}

Table 2. Integrated probabilities $\Delta P = \int_{v_{\min}}^{v_{\max}} (\mathrm{d}P/\mathrm{d}v)\mathrm{d}v$ per radiation length measured in three different intervals $(v_{\min}, v_{\max})$ compared with theoretical calculations for the sum of pair production (P), knock-on electron production (K), and two different formulae for bremsstrahlung, (B^{PS}) and (B^{TS}) (see formulae (1), (2), (3), and (5), respectively)

$(v_{\min}, v_{\max})$	$\Delta P_{\mathrm{measured}}$	$\Delta P_{P+K+B^{\mathrm{PS}}}$	$\Delta P_{P+K+B^{\mathrm{TS}}}$
$(0.01, 0.03)$	$(1.180 \pm 0.010_{\mathrm{stat}} \pm 0.080_{\mathrm{syst}}) \times 10^{-3}$	1.133×10^{-3}	1.150×10^{-3}
$(0.03, 0.12)$	$(3.130 \pm 0.060_{\mathrm{stat}} \pm 0.190_{\mathrm{syst}}) \times 10^{-4}$	3.039×10^{-4}	3.223×10^{-4}
$(0.12, 0.95)$	$(1.160 \pm 0.040_{\mathrm{stat}} \pm 0.075_{\mathrm{syst}}) \times 10^{-4}$	1.185×10^{-4}	1.472×10^{-4}
$(0.01, 0.95)$	$(1.610 \pm 0.015_{\mathrm{stat}} \pm 0.105_{\mathrm{syst}}) \times 10^{-3}$	1.556×10^{-3}	1.619×10^{-3}

tion (curve P in Fig. 7), the Bhabha formula for knock-on electrons (K) and with Petrukhin and Shestakov's (B^{PS}) and Tsai's (B^{TS}) calculations for bremsstrahlung processes.

4 Comparison of experiment and theory

The theoretical predictions are in very good agreement with the experimental results over the whole analysed range of fractional energy loss v from 0.01 to 0.95. It is worth noting that there are no free parameters in the comparison of theory and experiment, except for the very weak coupling. This is introduced by the requirement that the end-point of the experimental energy-loss distribution match the muon energy.

Since different processes dominate in different regions of v, theory and experiment can also be usefully compared in suitably chosen regions of the spectrum. The range of v analysed can be divided into the three intervals given in Table 2. About 55% of the integrated probability $\Delta P = \int_{v_{\min}}^{v_{\max}} (\mathrm{d}P/\mathrm{d}v)\mathrm{d}v$ in the first interval is due to the production of e^+e^- pairs; in the second interval 45% of the integral is due to knock-on electrons, and in the third interval the

dominant contribution (60%) comes from bremsstrahlung. The results obtained in all three intervals agree within one standard deviation (defined as the quadratic sum of statistical and systematic errors) with the theoretical predictions of Petrukhin and Shestakov for bremsstrahlung. The integrated probability value $\Delta P_{P+K+B^{\mathrm{TS}}} = 1.472 \cdot 10^{-4}$ in the region $v = 0.12 \div 0.95$ calculated with Tsai's description of bremsstrahlung is about 3.6σ (defined as the quadratic sum of statistical and systematic error) higher than the measured value $\Delta P = (1.160 \pm 0.040_{\mathrm{stat}} \pm 0.075_{\mathrm{syst}}) \cdot 10^{-4}$. This statement is illustrated further in Fig. 10, in which detailed comparison of the data and theory is shown. It can be seen that the results favour the description of bremsstrahlung by Petrukhin and Shestakov which predicts a lower probability of catastrophic muon losses.

References

1. ATLAS Collaboration, ATLAS Technical Proposal, report CERN/LHCC/94–43.
2. W. Stamm et al., Nuovo Cim. 51A (1979) 242.
3. K. Mitsui et al., Nuovo Cim. 73A (1983) 235.
4. W.K. Sakumoto et al., report UR-1209 (1991).
5. J.J. Aubert et al., Z. Phys. C10 (1981) 101.
6. Y. Tsai, Rev. Mod. Phys. 46 (1974) 815.
7. R. Kopp et al., Z. Phys. C28 (1985) 171.
8. R. Baumgart et al., Nucl. Instrum. Methods A258 (1987) 51.
9. W. Lohmann et al., CERN report 85–03 (1985).
10. R.P. Kokoulin and A.A. Petrukhin, Acta Phys. Acad. Sci. Hung. 29 Suppl. 4 (1970) 277.
11. A.A. Petrukhin and V.V. Shestakov, Can. J. Phys. 46 (1968) S377.
12. M.J. Tannenbaum, preprint CERN-PPE/91–134 (1991).
13. F. Ariztizabal et al., Nucl. Instrum. Methods A349 (1994) 384; E. Berger et al., report CERN/LHCC 95–44.
14. M. Lokajicek et al., ATLAS Internal Note TILECAL-NO-063 (1995).
15. Particle Data Group, Phys. Rev. D50 (1994) 1173.
16. S.R. Kel'ner and Yu.D. Kotov, Sov. J. Nucl. Phys. 7 (1968) 360.
17. H.J. Bhabha, Proc. Roy. Soc. A164 (1938) 257.
18. B. Rossi, High Enery Particles, Prentice-Hall, New York, 1952.
19. L.B. Bezrukov and E.V. Bugaev, Sov. J. Nucl. Phys. 33 (1981) 635.